TÜBİTAK

Turkish Journal of Physics

http://journals.tubitak.gov.tr/physics/

Research Article

Turk J Phys
(2021) 45: 378 – 389

doi:10.3906/fiz-2108-4

A simulation and experimental validation of third-order coma in nodal aberration theory with a Cassegrain telescope

Özgür KARCI*
TÜBİTAK Space Technologies Research Institute, Ankara, Turkey

Received: 05.08.2021 • **Accepted/Published Online:** 16.12.2021 • **Final Version:** 28.12.2021

Abstract: This study presents a simulation and experimental validation of third-order coma in Nodal Aberration Theory (NAT) with a custom-designed Cassegrain system. The Cassegrain system uses a piezo-driven flexure tool to align the telescope's secondary mirror with respect to the primary mirror. This alignment mechanism is also used to misalign the telescope's secondary mirror to induce the intentional aberrations. The third-order Fringe Zernike coma ($Z_{7/8}$) was simulated utilizing the Cassegrain telescope's real ray-trace model (e.g., in Code V) and analyzed for both the telescope's nominal aligned and misaligned states. The simulated aberration of third-order coma was induced utilizing the secondary mirror misalignments and measured interferometrically on a 5×5 mesh of field points on the telescope's focal plane. The experimental results were compared with simulation results, and we showed that the results are consistent with each other. Hence, we validated the shift of aberration field center (zero coma, or coma node) from the optical axis, where the third-order coma is linear with the field as predicted by NAT for the Cassegrain telescope. For demonstrating the stability and accuracy of the experimental results, a statistical analysis was conducted.

Keywords: Nodal Aberration Theory, Cassegrain telescope, third-order coma, telescope alignment, spaceborne telescopes, optical imaging systems

1. Introduction

Nodal Aberration Theory (NAT) is a crucial tool for emerging telescope technologies since it explains the properties of the aberrations for the misaligned/perturbed optical imaging systems. The invention of the theory by Roland V. Shack (University of Arizona) goes back to a photographic star plate image which was taken by a 90-inch Ritchey-Chrétien telescope of the Steward Observatory in Arizona in 1976. The astronomers brought the star plate to Shack to understand the residual aberrations on the gathered images; the images showed no coma induced by the misalignments. Instead, they have axial astigmatism. The investigation of the star plate showed two nodes of zero astigmatism on the image that the presence of two nodes (zeros) led Shack to name this new aberration behavior as "binodal astigmatism" and discovered NAT [1, 2]. The mathematics of NAT was developed by Shack and K. P. Thompson [3, 4] depending on Hopkins's wave aberration theory and the principles of aberration field center shifts through the misalignments developed by R. A. Buchroeder [5, 6]. Later, K. P. Thompson has developed NAT fully up to fifth-order aberrations [7–9]. Recently, K. Fuerschbach diversified

*Correspondence: ozgur.karci@tubitak.gov.tr

NAT for the new era of optics, freeform surfaces [10, 11]. Freeform surfaces are poised to revolutionize high-precision imaging systems, showing the noteworthiness of the theory [12].

NAT is thriving and has a well-established theoretical background, but experimental investigations are still in development. Latterly, experimental validation of third-order coma in NAT for a custom-designed, intentionally misaligned Ritchey-Chrétien (RC) telescope was explored by Zhao et al. RC is a two-mirror telescope type, which eliminates the third-order spherical and coma aberrations, and both third-order field curvature and astigmatism aberrations limit the performance of the RC telescope. The results gathered in this work for the RC telescope demonstrated field-constant third-order coma induced by the misalignments predicted by NAT [13]. "Binodal astigmatism", the root of NAT, was validated experimentally with a custom-designed, high-precision Cassegrain telescope for the first time by Karcı et al. [14, 15] lately. The field-linear dependence of third-order coma aberration for the Cassegrain system was also demonstrated experimentally for the on-axis position in this study. However, the shifted aberration field center of coma and its field-linear dependence has not yet been demonstrated.

This work explores a simulation and experimental validation of third-order coma in NAT with a custom-designed, high-precision Cassegrain system described in our previous works [16, 17]. The Cassegrain telescope utilizes piezo-driven, five-axis flexure stages to introduce the intentional misalignments to the secondary mirror to induce the aberrations. For a two-mirror Cassegrain telescope, spherical aberration is eliminated by design, but third-order astigmatism and coma limit the optical performance. Third-order coma shows linear field dependency. The aberration center of the coma is displaced on the image plane for the misaligned telescope as predicted by NAT. These predictions of the theory were simulated and validated experimentally for the Cassegrain telescope.

2. Theoretical background

The wave aberration expansion of third-order aberrations in vector form for a misaligned optical system can be written as in the following equation (note that bold depicts vector in this paper)

$$\begin{aligned} W &= \sum_j W_{040j}(\boldsymbol{\rho}\cdot\boldsymbol{\rho})^2 + \sum_j W_{131j}\left[(\boldsymbol{H}-\boldsymbol{\sigma}_j)\cdot\boldsymbol{\rho}\right](\boldsymbol{\rho}\cdot\boldsymbol{\rho}) + \sum_j W_{222j}\left[(\boldsymbol{H}-\boldsymbol{\sigma}_j)\cdot\boldsymbol{\rho}\right]^2 + \\ &\sum_j W_{220_j}\left[(\boldsymbol{H}-\boldsymbol{\sigma}_j)\cdot(\boldsymbol{H}-\boldsymbol{\sigma}_j)\right](\boldsymbol{\rho}\cdot\boldsymbol{\rho}) + \sum_j W_{311j}\left[(\boldsymbol{H}-\boldsymbol{\sigma}_j)\cdot(\boldsymbol{H}-\boldsymbol{\sigma}_j)\right]\left[(\boldsymbol{H}-\boldsymbol{\sigma}_j)\cdot\boldsymbol{\rho}\right] \quad (1) \end{aligned}$$

where $\boldsymbol{H}$ represents the field coordinate vector on the focal plane (normalized), $\boldsymbol{\rho}$ represents the pupil coordinate vector on the exit pupil (normalized), and $\boldsymbol{\sigma}_j$ represents the deviation in the aberration field center corresponding with surface j concerning the field center for the nominal system (or aligned). Each summation in the equation refers to one of the Seidel aberrations. The first term corresponds to spherical aberration, the second term correlates with coma, the third term correlates with astigmatism, the fourth one correlates with field curvature, and the fifth relates with distortion. W_{131} in Equation (1) represents the third-order coma wave aberration sum for the surface j, which can be defined in the following equation

$$W = \sum_j W_{131j}\left[(\boldsymbol{H}-\boldsymbol{\sigma}_j)\cdot\boldsymbol{\rho}\right](\boldsymbol{\rho}\cdot\boldsymbol{\rho}) = \left[\left(\sum_j W_{131j}\boldsymbol{H} - \sum_j W_{131j}\boldsymbol{\sigma}_j\right)\cdot\boldsymbol{\rho}\right](\boldsymbol{\rho}\cdot\boldsymbol{\rho}) \quad (2)$$

In Equation (2), the first term in summation represents the addition coming from the rotationally symmetric optical system, and it can be defined as

$$\sum_j W_{131j}\boldsymbol{H} = W_{131j}\boldsymbol{H} \tag{3}$$

The second term in summation of Equation (2) depicts the total surface displacement vectors on the focal plane associated with each surface. This sum gives a total, unnormalized displacement vector for the third-order coma on the image plane and can be written as

$$\boldsymbol{A}_{131} \equiv \sum_j W_{131j}\boldsymbol{\sigma}_j \tag{4}$$

A normalized vector, $\boldsymbol{a}_{131}$, is defined as

$$\boldsymbol{a}_{131} \equiv \frac{\boldsymbol{A}_{131}}{W_{131}} \tag{5}$$

where W_{131} represents wave aberration of the nominal system (or as designed) for third-order coma (for a Cassegrain system, in which coma is not corrected by design, $W_{131} \neq 0$), and Equation (2) can be rewritten as

$$W = W_{131j}[(\boldsymbol{H} - \boldsymbol{a}_{131}) \cdot \boldsymbol{\rho}](\boldsymbol{\rho} \cdot \boldsymbol{\rho}) \tag{6}$$

Equation (6) provides a resultant description of the third-order coma in a perturbed optical system in which the field dependency is described. Third-order coma is linear with the field when the optical system is misaligned (or perturbed from the nominal state), and the aberration center of the field is shifted on the focal plane, as seen in Figure 1.

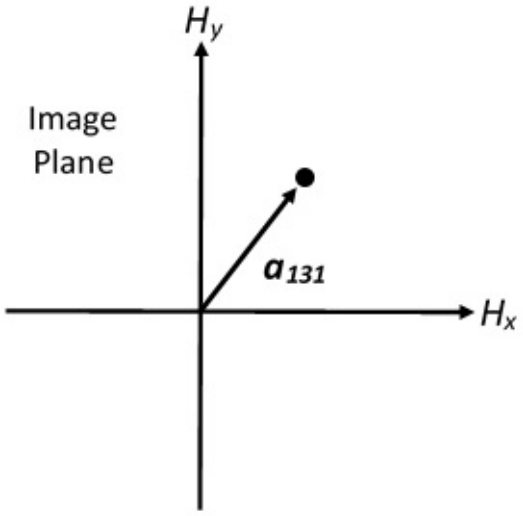

Figure 1. Schematic description for the field-linear third-order coma in a misaligned optical system. The aberration field center is displaced on the image plane, which is indicated by the vector $\boldsymbol{a}_{131}$.

For a Cassegrain system, the field-linear third-order coma can be visualized utilizing the Full Field Displays (FFD) function of Code V and Fringe Zernike coma ($Z_{7/8}$) is illustrated as given in Figure 2. The cones show the magnitude and direction of coma in FFDs. Figure 2a demonstrates the characteristic of a coma (by design) in which the node (point of zero coma) is on the optical axis. It is seen that coma depends linearly on the field of view. When a misalignment is introduced into the optical system, the node is displaced in the image plane and shifted away from the optical axis, as seen in Figure 2b. This aberration field is completely unchanged except that the field center decenter by a_{131}, proportional to the misalignment amount.

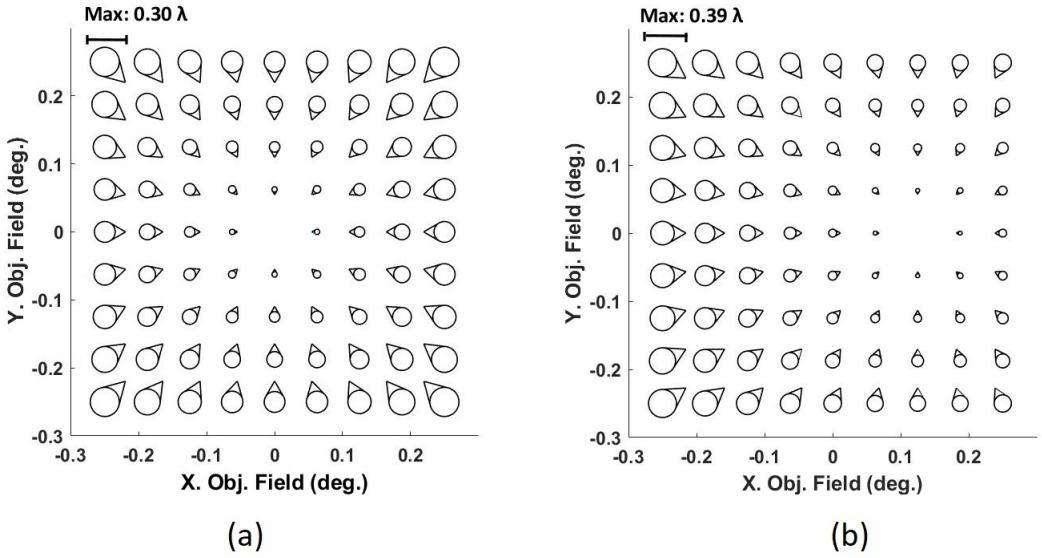

Figure 2. Full Field Displays (FFDs) graphs for Fringe Zernike coma ($Z_{7/8}$) in a Cassegrain telescope: (a) the telescope in an aligned state, and (b) the telescope is in a misaligned state in which the secondary mirror was misaligned -0.036 mm in the x-direction (XDE).

3. Cassegrain telescope

The design of the Cassegrain telescope is given in Figure 3. The telescope consists of a concave parabolic primary mirror (M1) and a convex hyperbolic secondary mirror (M2). The design has a rotationally symmetric optical design in which their optical axis coincides, and the secondary mirror obscured the primary mirror. M1 is defined as an aperture stop, which determines the telescope's aperture in the optical design. The radii of M1 is -1700 mm, and the radii of M2 is -300 mm. The conic constants for M1 and M2 are –1 and –1.737, respectively. The telescope's F-Number (F / #) is 12.7, and it is designed to be diffraction-limited for the ± 0.11 degree of the full field of view (FOV). The Cassegrain telescope's optical design specifications are given in Table 1.

The Cassegrain telescope was conceived according to the high-precision optomechanical considerations to meet stringent design requirements. An athermalized optomechanical structure comprises a mainframe, a primary mirror assembly (PMA), and a secondary mirror assembly (SMA). PMA includes a base plate attached to the mainframe, a light-weighted primary mirror, three glue pads, and three bipods. SMA consists of a secondary mirror, a spider, and piezo-driven flexure stages. SMA is connected to the secondary mirror ring employing three spider vanes that the whole assembly is

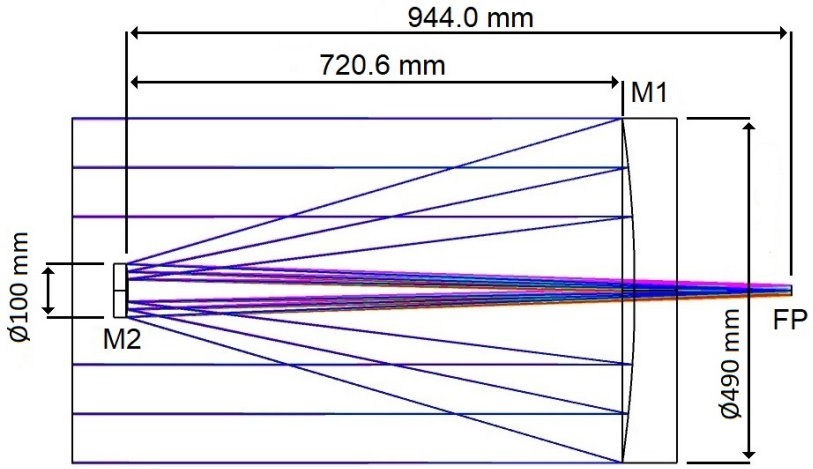

Figure 3. Schematic design layout of the Cassegrain system. M1 represents the primary mirror, M2 represents the secondary mirror, and FP represents the focal plane.

Table 1. Cassegrain telescope design specifications.

Feature	**Value**
Telescope aperture	490 mm
Reference wavelength	632.8 nm
FOV	± 0.11 degree
Effective focal length (EFFL)	6200 mm
Obscuration of M2 (linear diameter)	20%
Total telescope length	944 mm

connected to the mainframe utilizing six metering rods. The mainframe, spider, spider vanes, and secondary mirror ring are made of high-strength aluminum. The metering rods, mirror supports are made from the low-thermal expansion Invar. The mirrors are made from Zerodur glass-ceramic (e.g., Schott AG, Class 1, Germany). SMA has a piezo-driven (e.g., PZA 12 actuators, Newport Corp., USA), five-axis flexure tool (Tip/Tilt, X, Y, and Z) for fine adjustment of M2 concerning M1 during the alignment process. This high-precision alignment tool was also utilized to introduce the misalignments to the telescope's secondary mirror to generate aberrations. All the design and realization details of the telescope were given in our previous study [16].

4. Experimental setup and simulation results

4.1. Experimental setup and telescope alignment

The experimental setup is based on the auto-collimation two-pass design layout, which comprises the telescope, reference flat mirror, an interferometer, as seen in Figure 4. In this configuration, a Fizeau phase-shifting interferometer (e.g., Zygo Corp., DynaFiz, USA) is confocal to the telescope and reflected by the secondary mirror and the primary mirror, respectively. Then, the output light beam of the telescope is reflected by a reference flat mirror (e.g., QED Optics, USA) and follows the same path

through the interferometer for producing the interference for measurement. The interferometer was put on a customized, five-axis manual stage to move the focus of the interferometer on the simulated field points for measurements. The reference flat mirror is integrated into a hub controlled by a two-axis motorized stage (Tip/Tilt) to reflect the telescope output light beam for the field points. The entire setup was placed onto an optical table with self-balancing vibration isolation stages (e.g., Newport Inc., S2000A, USA), as seen in Figure 5.

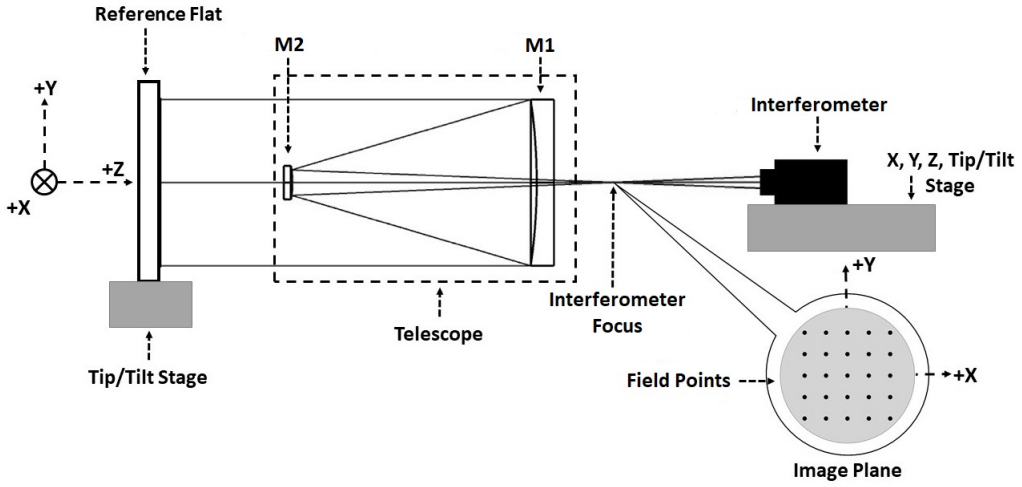

Figure 4. Schematic design layout of the two-pass interferometric measurement setup in which the interferometer is confocal to the telescope. The field points are depicted as a 5×5 grid on the image plane.

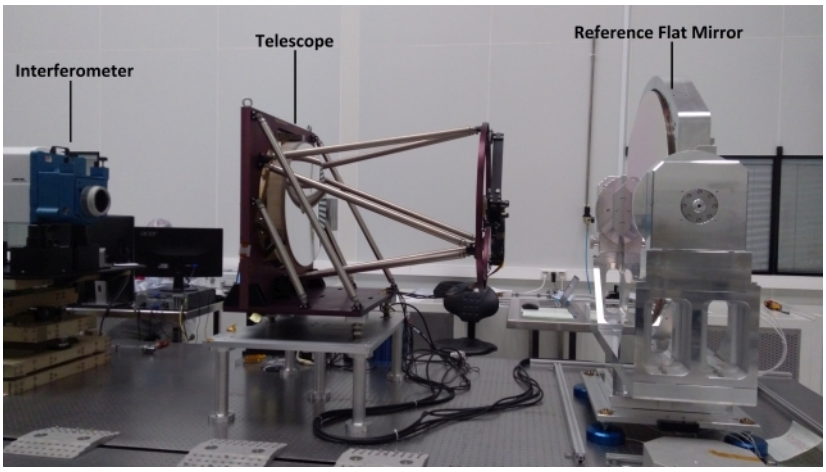

Figure 5. Cassegrain telescope in auto-collimation test setup configuration placed onto the optical table.

A sensitivity matrix of the optical system in a real ray trace model (e.g., Code V) was generated to perform the alignment of the Cassegrain system. For this purpose, the secondary mirror was perturbed according to the degrees of freedom in design (Tip/Tilt, X, Y, and Z), and the Fringe Zernike terms (Z_{5-9}) for third-order aberrations were recorded. In general, for two-mirror telescope systems, the secondary mirror, which is the most sensitive element to the aberrations, is aligned with

respect to the primary mirror. The alignment was performed for the on-axis field of the telescope (Field 0), the secondary mirror was tuned for decreasing the third-order Fringe Zernike terms in a predetermined manner. A comprehensive description of the alignment of the telescope was studied in our earlier work [16]. The alignment process resulted in 0.02 wave RMS wavefront error (WFE) at 632.8 nm, as illustrated in Figure 6 before the field tests.

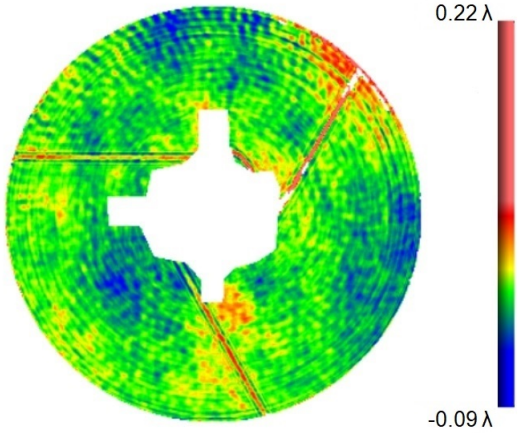

Figure 6. Phase-shifting interferometer data (wavefront error) for the aligned Cassegrain telescope in which the central part of the data shows the secondary mirror's obscuration and the piezo stages ($\lambda =$ 632.8 nm).

4.2. Simulation results for third-order coma

Simulations of the third-order coma in NAT were conducted utilizing the Cassegrain telescope's real ray-trace model in Code V. The corresponding third-order coma 7th and 8th Fringe Zernike Coefficients (ZFC) were gathered using the optical design software's Wavefront Map Analysis function. The Zernike terms quantify the magnitude of third-order coma according to Equation (7). Initially, the associated interferograms for a 5×5 mesh of field points, which is given in Table 2, were generated utilizing a customized Matlab code for the nominal state of the telescope (aligned or as designed). The interferograms are illustrated in Figure 7a. Later, the secondary mirror was misaligned in the x-direction (XDE) with –0.036 mm. Then, the interferograms are given in Figure 7b were generated for the misaligned state. As seen from Figure 7b, the coma node was displaced on the image plane from the optical axis by the misalignment of the secondary mirror. The interferograms show the magnitude and orientation of third-order coma for the 5×5 mesh of field points for both states of the telescope. The amount of the misalignment was chosen to displace the coma node in the measurable field of view by the interferometer. The data at the corners were excluded from the analysis since the experimental setup could not acquire data for the fields located at the corners. This was caused by the obscuration of the primary mirror inner hole dimension (or corner field points are out of the telescope's field of view).

$$|Z_{7/8}| = \sqrt{Z_7^2 + Z_8^2} \tag{7}$$

Table 2. The simulated field positions on the image plane as a 5×5 grid.

(–0.250°, 0.250°)	(–0.125°, 0.250°)	(0°, 0.250°)	(0.125°, 0.250°)	(0.250°, 0.250°)
(–0.250°, 0.125°)	(–0.125°, 0.125°)	(0°, 0.125°)	(0.125°, 0.125°)	(0.250°, 0.125°)
(–0.250°, 0°)	(–0.125°, 0°)	(0°, 0°)	(0.125°, 0°)	(0.250°, 0°)
(–0.250°, –0.125°)	(–0.125°, –0.125°)	(0°, -0.125°)	(0.125°, –0.125°)	(0.250°, –0.125°)
(–0.250°, –0.250°)	(–0.125°, –0.250°)	(0°, -0.250°)	(0.125°, –0.250°)	(0.250°, –0.250°)

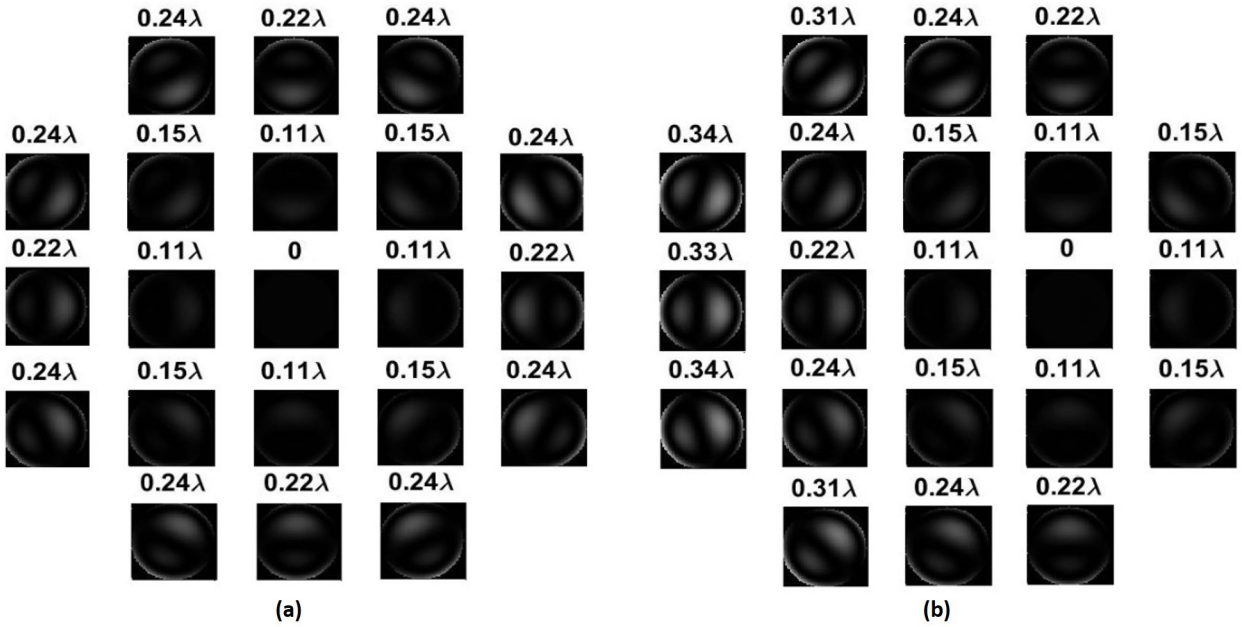

Figure 7. Simulated interferograms of Fringe Zernike coefficients ($Z_{7/8}$): for the third-order coma (a) aligned state, (b) misaligned state. M2 was misaligned -0.036 mm in the x-direction (XDE), (λ= 632.8 nm).

5. Experimental Results

Interferometric tests were carried out for the field points simulated in Table 2, and the associated interferograms shown in Figure 8 were gathered. The interferometric raw data were analyzed using custom Matlab codes to calculate each field point's Fringe Zernike coma ($Z_{7/8}$). The results are presented in Figure 9, which shows the consistency of the experimental results with the simulations. As seen in Figure 9, the third-order coma aberration field center (or node) is displaced from field points of (0°, 0°) to (0.125°, 0°) on the image plane, and the third-order coma is linear with the field at this new field center as simulated. In addition, the results showed that there is an insignificant difference between the two results, and the amount of difference was in the one to five 100th of a wave (λ = 632.8 nm). The primary source of error was the manual positioning of the interferometer focus through the field points on the image plane. The other reason for the error was the SMA alignment mechanism used to introduce the simulated misalignment to the secondary mirror.

For the validation of experimental data, the locations of the third-order coma node were calculated from both the experimental data and analytically utilizing the Equations (2)–(6) as seen in

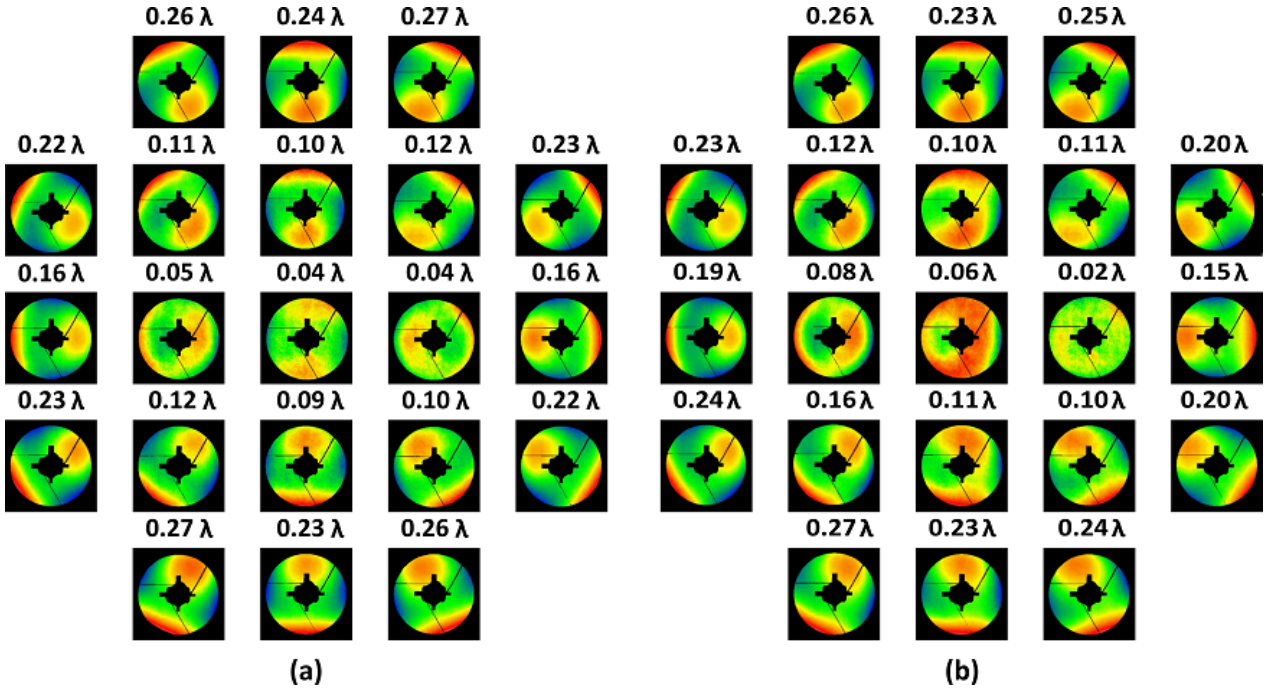

Figure 8. The raw data for interferograms by experiments on the field points: (a) aligned state, (b) misaligned state. RMS WFE of each data is given on each interferogram data (λ= 632.8 nm).

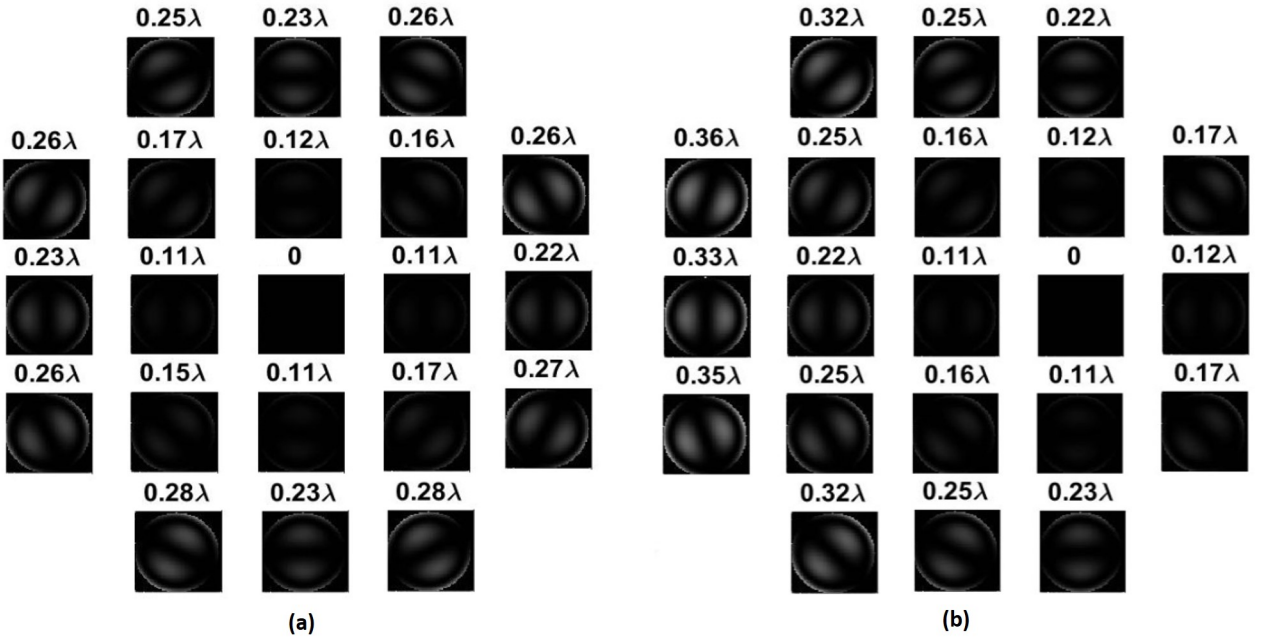

Figure 9. Interferograms of Fringe Zernike coma ($Z_{7/8}$) from the processed experimental data: (a) aligned state, (b) misaligned state (λ= 632.8 nm).

Table 3. The results are consistent with each other, and they are within two-thousandths of a degree. Therefore, the results validate NAT experimentally for third-order coma.

Table 3. Calculations of the third-order coma node locations.

Parameter	X-Component	Y-Component
Analytically (degree)	0.1277	0
Experimentally (degree)	0.1250	0

The interferometric measurements were analyzed statistically to see the impacts of the environment where the experiments were conducted, such as vibration, air turbulence, and temperature, on the stability and accuracy of the experimental results. Therefore, we performed eight consecutive measurements at a single field point (e.g., 0.125°, –0.250°) in the telescope's misaligned state. Figure 10a shows the variation of four variables: Fringe Zernike coma terms (Z_7) and (Z_8), pair of Fringe Zernike coma ($Z_{7/8}$), and the RMS WFE are given in a line chart for eight consecutive measurements. The deviation from the mean values for (Z_7), (Z_8), and RMS WFE are illustrated in Figure 10b. In the analysis, the standard deviations for the variables (Z_7), (Z_8), ($Z_{7/8}$), and RMS WFE were calculated to be 0.001 waves at 632.8 nm. The results show both the stability and accuracy of the measurements.

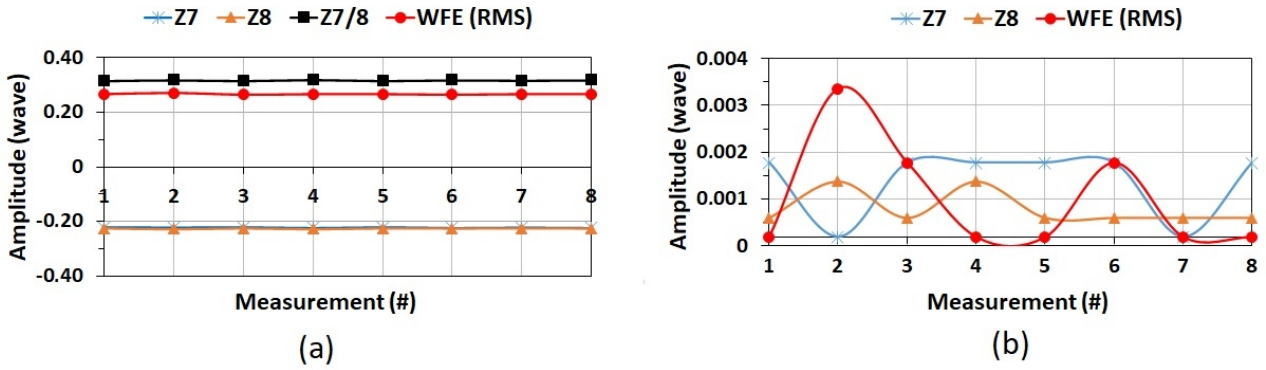

Figure 10. Graphs for the statistical analysis (a) amplitudes for consecutive measurements, and (b) deviations from the means (λ= 632.8 nm).

6. Conclusions

The simulations and experimental validation of third-order coma in Nodal Aberration Theory were presented for a Cassegrain system for the first time. The induced third-order coma aberration by intentional misalignments was simulated and measured on a 5×5 grid of field points utilizing an interferometer. The simulations and experimental investigations showed that the secondary mirror misalignment in a Cassegrain system displaces the node of third-order coma on the image plane from the optical axis, and the coma shows field-linear dependency at this new node location. For the experimental validation of third-order coma in NAT, the location of the coma node was calculated utilizing experimental data and analytically. The results are consistent with each other, within two-thousandths of a degree, which validates the theory. Statistical analysis was also exerted to show both

the stability and accuracy of the measurements. The analysis results showed that the environmental conditions had an insignificant impact on the uncertainty. The major limiting factor was the manual adjustment of the interferometer focus through the field points on the image plane, and the uncertainty was in the 100th wave magnitude. As the theory foresees, the third-order coma node is displaced from the optical axis on the image plane by misalignment. It shows field-linear dependency for a two-mirror Cassegrain telescope.

Acknowledgments

This work was partially supported by Fulbright Association (FY-2019-TR-PD-06). The author thanks the University of Rochester and Prof. Jannick P. Rolland for their hosting during his Fulbright fellowship. The author also thanks Synopsys Inc. for supplying a free Code V academic license.

References

[1] J. P. Rolland, A. Bauer, K. Fuerschbach and K. P Thompson, "Roland V. Shack's discovery of nodal aberration theory, the expansion into the aberrations of freeform optics, and impact in optical design" Proceeding of SPIE **11479** (2020) 72-79.

[2] K. Thompson, "Description of the third-order optical aberrations of near-circular pupil optical systems without symmetry", Journal of the Optical Society of America A **22** (2005) 1389-1401.

[3] K. P. Thompson, "Aberration fields in tilted and decentered optical systems", PhD Thesis, University of Arizona, USA (1980).

[4] R. V. Shack and K. P. Thompson, "Influence of alignment errors of a telescope system on its aberration field", Proceeding of SPIE **0251** (1980) 146-153.

[5] R. A. Buchroeder, "Tilted component optical systems", PhD Thesis, University of Arizona, USA (1976).

[6] K. P. Thompson, T. Schmid, O. Cakmakci and J. P. Rolland, "Real-ray-based method for locating individual surface aberration field centers in imaging optical systems without rotational symmetry", Journal of the Optical Society of America A **26** (2009) 1503-1517.

[7] K. P. Thompson, "Multinodal fifth-order optical aberrations of optical systems without rotational symmetry: spherical aberration", Journal of the Optical Society of America A **26** (2009) 1090-1100.

[8] K. P. Thompson, "Multinodal fifth-order optical aberrations of optical systems without rotational symmetry: the comatic aberrations", Journal of the Optical Society of America A **27** (2010) 1490-1504.

[9] K. P. Thompson, "Multinodal fifth-order optical aberrations of optical systems without rotational symmetry: the astigmatic aberrations", Journal of the Optical Society of America A **28** (2011) 821-836.

[10] K. Fuerschbach, J. P. Rolland and K. P. Thompson, "Theory of aberration fields for general optical systems with freeform surfaces", Optics Express **22** (2014) 26585-26606.

[11] A. Bauer, E. M. Schiesser and J.P Rolland, "Starting geometry creation and design method for freeform optics", Nature Communications **9** (2018) 1-11.

[12] J. P. Rolland, M. A. Davies, T. J. Suleski, C. Evans and A. Bauer *et al.*, "Freeform optics for imaging", Optica **8** (2021) 161-176.

[13] N. Zhao, J. C. Papa, K. Fuerschbach, Y. Qiao and K. P Thompson *et al.*, "Experimental investigation in nodal aberration theory (NAT) with a customized Ritchey-Chrétien system: third-order coma", Optics Express **26** (2018) 8729-8743.

[14] Ö. Karcı, E. Arpa, M. Ekinci and J. P. Rolland, "Experimental investigation of binodal astigmatism in Nodal Aberration Theory (NAT) with a Cassegrain telescope system", Optics Express **29** (2021) 19427-19440.

[15] Ö. Karcı, E. Arpa, M. Ekinci M and J. P. Rolland, "Experimental investigation of third-order binodal astigmatism in Nodal Aberration Theory (NAT) with a Cassegrain system", Proceeding of SPIE **12078** (2021) 1-7.

[16] Ö. Karcı and M. Ekinci, "Design of a high-precision, 0.5 m aperture Cassegrain telescope", Applied Optics **59** (2020) 8434-8442.

[17] M. Ekinci M and Ö. Selimoğlu, "Development of a 0.5 m clear aperture Cassegrain type collimator telescope", Proceeding of SPIE **9912** (2016) 1504-1516.